Structures 64 (2024) 106592

Contents lists available at ScienceDirect

Structures

journal homepage: www.elsevier.com/locate/structures

Integrating R-funicularity, local stability and inter-panel constraint assessment for discrete timber shell construction design

Sam Wilcock [a,*,1], Han Fang [a,2], Mehmet R. Dogar [b,3], Ornella Iuorio [c,4]

[a] School of Civil Engineering, University of Leeds, Leeds LS2 9LG UK
[b] School of Computing, University of Leeds, Leeds LS2 9JT UK
[c] Department of Architecture, Built Environment and Construction Engineering, Politecnico di Milano, 20133 Milan Italy

ARTICLE INFO

Keywords:
Shell structures
Rigid-block analysis
Laser cutting
Dry stacking
3D printing
Timber design
Digital assembly

ABSTRACT

Timber shell structures are material efficient over large spans, and environmentally friendly due to the renewable nature of the material. In realising such structures, digital fabrication and assembly techniques provide new opportunities for the accurate conversion of complex digital designs into real components, allowing the generation of interlocking shell forms. Supporting falsework structures for shell construction present issues as a high waste factor in their assembly, due to their often single-use, and highly custom nature. Additionally, such segmented shells often rely on adhesives or additional fixings to constrain parts, reducing the potential for disassembly and reuse. This work presents a design approach, developed to demonstrate the use of dovetail style integral joints for maintaining structural stability through the assembly process, mitigating the need for falsework. The proposed approach is based on making use of stability assessments, funicularity measures and geometrical analysis of part interfaces to understand the behaviour of designed structures in an assembled state, during assembly, and how parts may be inserted into each other. Relaxed funicularity of full shell designs is quantified to assess fully assembled loading mechanisms, whereas the coupled rigid-block analysis (CRA) is used to assess the stability during assembly and is validated by comparison to physical models. Using the part-part interface geometry information and panel topology, inter-panel constraints are also assessed for both dovetail and finger joints. The developed interlocking joints are shown to aid funicularity by improving tensile capacity. Comparisons are made between inter-panel constraints and stability analysis data to show the relationship between interface geometry and stability. Together, these three techniques are shown to provide complementary early-stage design feedback to aid in generating feasible, discrete shell constructions.

1. Introduction

Well-designed shell structures offer many benefits for structural designers, the most notable being relatively low material usage over large footprints due to their efficient membrane-dominated load-carrying mechanism. Traditionally, inherently stable geometries were found through the observation of the shapes formed by hanging chains, soap bubbles and other physical models. More recently, computational form-finding techniques allow the exploration of a vast set of geometries, for which the loading path falls fully within the shell thickness [1,2]. Such designs are under pure compression without bending moments [3], providing their own stability without need for external supports.

In thin structures, it is also currently commonplace to form-find optimal shapes for their specific load conditions through the use of computational dynamics simulation [4]. Such simulation tools are now integrated into the computer-aided design toolbox alongside parametric software such as Grasshopper® [5], which allows the application of algorithmic rules to generate geometries. The forms found are well-suited to continuous shells such as those made from concrete, as those by Torroja, Candela, Nervi and Isler [6]. Recently, driven by the complexities of formwork construction and the benefits of prefabrication of shell elements for onsite assembly, research has increasingly

* Corresponding author.
E-mail addresses: s.wilcock@leeds.ac.uk (S. Wilcock), h.fang1@leeds.ac.uk (H. Fang), m.r.dogar@leeds.ac.uk (M.R. Dogar), ornella.iuorio@polimi.it (O. Iuorio).
[1] 0000-0002-8353-6219.
[2] 0000-0001-7552-8799.
[3] 0000-0002-6896-5461.
[4] 0000-0003-0464-296X.

https://doi.org/10.1016/j.istruc.2024.106592
Received 31 October 2023; Received in revised form 4 May 2024; Accepted 15 May 2024
Available online 28 May 2024

focused on segmented shell design. Segmented shells can be generated by stereotomic tiling of continuous shells into cut voussoirs, maintaining their curved interior (intrados) and exterior (extrados) surfaces [7] or approximating them with planar surfaces [8]. The Armadillo vault, for instance, used a combination of curved and planar interface surfaces, with only the curved interfaces supporting the loads [9]. The tessellation employed relied heavily on manual design but demonstrated the generation of segmented shell forms, the ease of assembly using prefabricated elements and the application of planarization to extrados.

It is often beneficial instead to design elements with parallel planar intrados and extrados, for the use of materials such as sheet glass or timber stock. Design of planar polygonal architecture requires approximating the original geometry through planarization methods. The variational tangent plane intersection (VTPI) technique is one optimisation-based method of interest [10] where each polygonal face is assigned a parallel plane, which may change orientation and central position. By assigning energies to neighbouring panel edge distances and vertices, the mesh can be relaxed towards a lower energy state, and panel vertex positions and orientations can be found that satisfy planarity and neighbour edge matching requirements. Alternative planarization techniques exist such as agent-based methods, which are being explored by ICD Stuttgart [11] which are performant yet more complex to implement.

Hexagons are commonly used for panelling, due to the quality of the approximations to the original design surface they can provide [12]. In these approximations and their planarization, heptagons and pentagons commonly arise, leading to the surface structure being described as hexagon-dominant meshing [10]. Using hex-dominant meshes as the basis for 3D voussoirs can lead to completely kinematically constrained configurations for dome-like structures, which do not require additional fixing once assembled. Sliding failure is however likely at openings and edges without additional constraint [13]. Additionally, the generation of these 3D voussoirs can lead to conflicts between the different design goals, e.g. the matching of interface edges, planarity, shell curvature and minimum panel sizes. Schwinn et al. (2023) have recently used agent-based modelling to find appropriate geometry within design constraints [14], which is performant yet complex to implement. The ECHO shell project by Iuorio et al. (2019) outlined a design process focusing instead on the use of form-finding software as an optimisation tool for the generation of hex-dominant planar panels [15]. However, there was little consideration for edge interface geometry due to the very thin nature of the panels. Hence, the use of form-finding as optimisation for thicker voussoir generation is open to exploration.

Beyond geometric design, it is imperative to be able to analyse the stability of designed structures. Recent work by Gabriele et al. (2018) [16] focuses on quantifying how close shell geometry is to funicularity. Their R-funicularity approach gives a flexible definition of compression-dominated structures, based on the ratio of local bending to normal forces. Shell designs within funicularity limits are globally stable. Hence, they are stable once fully assembled. However, traditionally scaffolding or falsework supports are required during the construction, to temporarily support bending moments which may arise before the full structure is in place. Formwork tailored for supporting the assembly of a bespoke shell structure is attributed to a high proportion of project cost and material waste, with one review citing formwork being responsible for between 25 % and 45 % of the overall material waste [17]. Therefore, reducing formwork usage is of paramount importance to develop systems with lower carbon footprint.

Previous works have taken advantage of reconfigurable formworks, whether through mechatronic actuation [18] or mechanical design [19]. However, these studies primarily deal with the manufacture of concrete continuum shells. In the case of segmented shells, others have made use of robot manipulators as temporary supports as well as construction agents, where multiple robot arms are used to provide scaffolding in key locations whilst humans or other robots continue the shell assembly [20,21]. Such operations however require high precision of calibration to understand the relative locations of the robots, and often require human intervention as well as large amounts of sensing data. In purely mechanical designs, the ICD Stuttgart research group provided a key development with the BUGA wood pavilion in 2014 [22], a successfully built 200 m^2 structure constructed from a cassette system. The cassette system used digitally fabricated hollow elements with hex-dominant panelling, fixed together with adhesives, nuts and bolts [23]. Notably, the system is supported during assembly by the connections between panels, yet is still reliant on some point-support scaffolding. Additionally, it was noted that the use of the fixing bolts constituted a large proportion of the assembly time. Others have designed more reversible fixing techniques for hex-dominant panels, with the ECHO shell making use of bespoken 3D-printed mechanical connections to carry the bending moment during the construction stage [24]. Also this shell is designed with the intent of minimising formwork, yet still requires some small degree of support during assembly as well as additional labour to apply the joint fixtures. Research from Robeller et. al at EPFL (2017) used quadrilateral cassette designs with interlocking integral mechanical timber tabs to interlock elements between the cassettes [25], although adhesives and mechanical fixings were also applied. Their Recycleshell design alternatively used custom wooden bowtie fasteners which were inserted during assembly [26]. Both the BUGA pavilion and the ECHO shell clearly demonstrate the potential for the use of external joints and fixings to resist bending moments in shells during assembly. However, the use of support structures is still required. The mechanical designs of EPFL demonstrate the potential for integrated mechanisms to hold elements together, yet still requires additional labour to ensure cohesion between cassettes. Clearly, the reliance on additional fixings increases construction time. A more efficient alternative could be to design locally stable structures, i.e. structures which can fully support themselves during the assembly process, without the need for any external scaffolding. Robeller's work clearly suggests that this is possible using integrated joint geometry, although until now a purely integrated slotted joint manufactured as part of the panel has not been demonstrated. However, this would require estimation of the stability, deflections and stresses present during the shell assembly.

The work, presented in this paper, presents a new approach for the design and construction of shell structures which remain stable during assembly. Expanding on the state of the art, it is sought to mitigate the need for external scaffolding or the need for semi-permanent fixings.

In designing self-supporting assemblies, it is important to be able to verify the stability of the structure throughout construction. Finite element analysis (FEA) is often used as an advanced structural analysis tool. It allows modelling of complex geometries, fine control over material properties and accuracy. It is however computationally expensive; accuracy comes at the cost of increasing mesh resolution and computation time. In the design of masonry shells, some authors have made use of physics-based game engines such as Bullet [27] and PhysX [28] for rapid testing of structural stability, however physics engines require careful parameter tuning if they are to be stable [29], due to accumulation of estimation error. Alternative mathematical models for rigid bodies have been proposed, primarily based on the safe theorem of limit analysis by Heyman [30]. The theorem states that for a statically indeterminate structure, if an admissible stress state can be found within the structure which is in equilibrium, then the structure will be stable. The rigid-block equilibrium (RBE) analysis is a formulation of such an equilibrium problem which frames it as an optimisation [31–33], minimising the number of contact forces and using equilibrium and friction relations as constraints, based on prior work by Livesley [34]. Based on this formulation, Kao et al. wrote software tools to combine the rigid block model with a kinematic approach, named the coupled rigid-block analysis (CRA), which added virtual rigid-body motion [35]. The method was demonstrated to correctly assess the stability of the Block Group's fully assembled Armadillo shell [9], along with local stability assessment of assembly stages for a bridge model, however until now, there has been limited work applying the technique to stages of shell

assembly [36].

In addition to predicting whether a structure will be stable, it is also important to know whether it will be feasible for assembly. Parts should be realistic to assemble, and not merely be possible within computer graphics. Elements can be designed in CAD with infeasible states, with elements that block their insertion into each other, and would be impossible to physically assemble. For example, two elements may be designed to slide together in a way that they cannot realistically be built, due to a third part blocking their insertion. This is a common problem in assembly design which has been studied as part of the assembly sequencing problem, found originally in research on computer graphics [37]. Assembly sequencing is reviewed extensively by Jiménez [38], and has been utilised for the robotic planning of motions to construct assemblies [22,39]. Using geometric data from parts, and by understanding how part interfaces contact each other, it is possible to find feasible insertion directions for elements. It is also possible to use these locally unconstrained direction vectors to then search for potential assembly sequences, or to discover that an assembly is infeasible for real-world construction due to blocking relationships with neighbours. Huang et al. [40] used assembly sequencing for the design and robotic assembly of structurally stable frame structures, however the focus was on frame elements such as rods rather than volumetric panels. Other authors have utilised computational dynamics engines to undergo exhaustive testing of possible disassembly sequences [28], which again can suffer from issues of numerical instability. In this work, the blocking relationships between solid panels are explored, used to verify the feasibility of a shell assembly. Additionally, joining techniques which exhibit high kinematic freedom are shown to be unstable using rigid body analysis.

2. Scope, novelty and structure of the paper

In this work, a segmented shell design approach is outlined, and a novel integrative approach is proposed which combines the use of R-funicularity, coupled rigid-block analysis, and inter-panel constraint assessment. This paper demonstrates through mathematical, numerical and prototyping analysis that the stability of the structure throughout the entire assembly process can be described, and the relative potential interactions of neighbouring panels can be given looking at geometric constraints. In section 3.1, the design process of a planar-panelled discrete shell structure is described, highlighting the techniques for developing a funicular approximation to an intended geometry, then a related panelled structure is developed using an innovative method of converting mesh geometry to surfaces which are easier to work with for panelling. In section 3.2, a joint design and propagation technique is described which can be applied between panels to form insertional joints. Three analysis aspects are then described relating to the fully assembled, partially assembled and local part kinematic scales. In section 3.3, the method of using R-funicularity to post-process FEA results is described, for assessing the funicular stability of the fully assembled structure. In section 3.4, the CRA analysis is introduced as a tool for understanding the stability of the partially assembled structure through rigid block mechanics. In section 3.5, local part-part relationships are explored through geometric inter-panel constraint assessment, to ensure that parts can be feasibly assembled without being blocked. Some initial analyses are introduced through Section 3 to better demonstrate their usage and setup. In Section 4, results of the analysis on the final designed structure are demonstrated, with reflection on their significance. The R-funicularity of the final design is described, showing that the joints infer stability by estimating the tensile strength that they provide to a shell (Section 4.1). Numerical analysis of the shell design through coupled rigid block analysis are provided and validated, in order to demonstrate the stability of the structure during its assembly (Section 4.2), and the geometric inter-panel constraints are assessed for two different joint styles to compare the kinematic effects to the stability data (Section 4.3). Finally, in Section 5, the inter-related aspects of these analyses are discussed, and the benefits of their use as early-stage design tools are highlighted. The combination of the linear-elastic FEA post-processing of R-funicularity, and the rigid mechanics modelling of CRA is a novel application which explores the effects of loading both within the body of the shell and at panel interfaces. The application of joint kinematics through geometric relationships is well-understood, however has not previously been linked to the stability of a structure, and is shown to be an early predictor in structural design for integrally joined panels.

3. Methods

The stability of shell structures is well studied with respect to continuous or gridshell forms [41] but is less well defined for segmented shells. Such structures undergo displacements and stresses which can arise due to constitutive properties such as material strength and density, and due to interactions between segments which make modelling more complex. The aim of the current study is to connect the stability of tessellated structures to their geometric design, and to understand the stability both in the fully and partially assembled states whilst ensuring feasible assembly. To achieve this, a case study approach is used. Specifically, a hexagonal segmented shell structure with interlinked dovetail jointed panels is developed, using a novel application of joint propagation based on liaison matrices. Numerical analyses are developed to present the R-funicularity for the shell case, and to visually show the effects of panelling on funicularity with a new graphical representation technique. The numerical model of coupled rigid-block analysis is applied to a section of the shell and is validated using a 3D printed prototype by comparison of displacement results, demonstrating its potential as a tool in understanding construction stages for segmented shells.

3.1. Case study design

In designing shells, a design intent is often specified. Such designs could be free-form, in which case there is little chance that the shell is funicular. To adjust such designs towards a funicular solution, an approach is described to convert a free-form design into a similar form-found one (Fig. 1). A base surface model seen in Fig. 1a, of footprint 3.2 $\times$ 1.6 m was conceived, with a height of 1.9 m, based on a section of a sphere.

Parametric design tool Grasshopper's [5] physics plugin Kangaroo [42] is used to optimise mesh data-structures based on energy goals. A desired input shell in the form of a non-uniform rational B-spline (NURBS) surface was first converted to a mesh data structure, and stiffness was applied to the mesh edges by setting a goal to minimise edge lengths, simulating material stiffness. The base nodes at $z = 0$ have constraints as pin-support boundary conditions, while to create a thrust and generate pressure on the shell, a vertical load is applied upwards through shell nodes, parallel to the Z axis of the design. Treating these goals as energy criteria with different weights associated to them, the design is subsequently optimised to minimise the energy within the structure through a method similar to dynamic relaxation [3,43] to give a form-found geometry with zero thickness. The design should be approaching funicularity as the stress is concentrated longitudinal to the mesh edges, dictating purely membrane loading.

To rationalise the designed continuous shell into a discrete panelled structure, there are numerous techniques of generating repeating tessellations. Tilings have been well-defined in planar rectangular regions [44], and a standard technique for application to 3D surfaces is to re-parameterise the tile vertices and edges on a planar rectangle into a deformed NURBS rectangular grid. In the more general free-form case, it is possible to tile surfaces through stitching together NURBS surfaces [45], however this still relies on the use of quadrilateral patches. CAD software has built-in functions for the approximation of NURBS surfaces into meshes (which were used here for converting the initial free-form design into a suitable mesh for form-finding), however the inverse

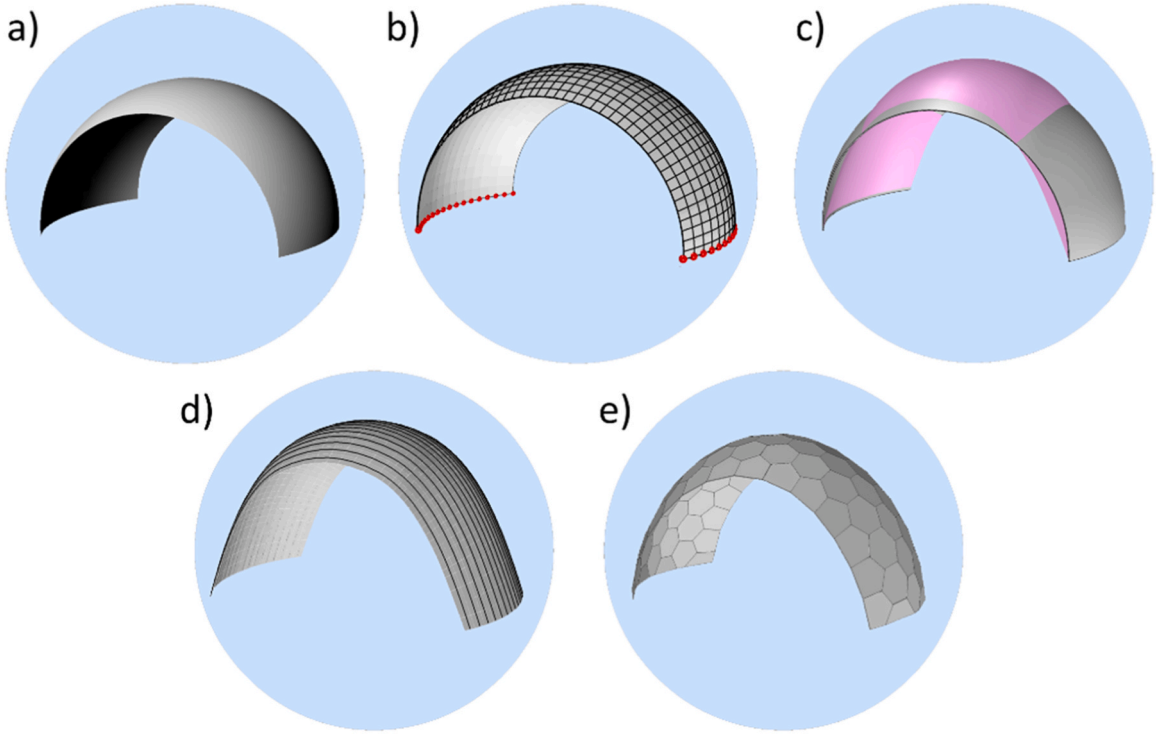

Fig. 1. Design stages for the shell. **a)** Initial form intent. **b)**. Meshing, and selecting the restrained mesh nodes (in red). **c)** Form-finding to give funicular geometry. **d)** Conversion to loft-fitted surface. **e)** Panelling and planarizing. (For interpretation of the references to color in this figure legend, the reader is referred to the web version of this article.)

operation has limitations. NURBS surfaces describe single, untrimmed shapes with 4 edges and a rectangular UV structure, which is a restrictive requirement compared to meshes.

A solution was developed which approximates the form-found mesh geometry back into an untrimmed surface. Contour curves were generated across the mesh, and broken lines were discarded. The desired effect is achieved by fitting a loft to these lines, which is inherently an untrimmed surface (see Fig. 2). It should be noted that this procedure will not work for most designs, while it is suitable for those with 4 edges and a roughly quadrilateral design due to the inherent nature of single NURBS surfaces.

Using this NURBS approximation to the form-found relaxation of design intent, the design can now be tiled into a hex-dominant pattern. Hexagons are selected due to the properties of hexagons to provide high level of approximation of the base surface and the kinematic constraints they can infer, as previously discussed. There are numerous software tools designed for this purpose – in this case, the HexDivide component from Petras Vestartas' open source Ngon plugin [46] was used. Once tiled, a planarization with similarities to VTPI optimisation was simulated using Kangaroo in an additional form-finding stage. This acts to relax the mesh to planarize its faces, following a similar procedure to that employed for the ECHO shell [15]. The tile edges have length constraints applied to keep them close to their original sizes, and coplanar goals are set on the panel vertices to optimise towards planar panels. A low-energy objective is a local set of points which are perfectly planar, and the Kangaroo optimisation moves iteratively towards these states, and if successful a planar tessellated geometry is found. This procedure is not, however, guaranteed to find a stable solution. The optimisation-based planarization can optimise early in local minima due to the conflicts between goals, finding completely planar or otherwise inappropriate geometries. This is mitigated through gradually increasing the planarization goal weight, preventing the planarization goal from dominating the optimisation. Once the procedure converges on a set of planar panels that fit the structure, extrados are subsequently generated in a process detailed below.

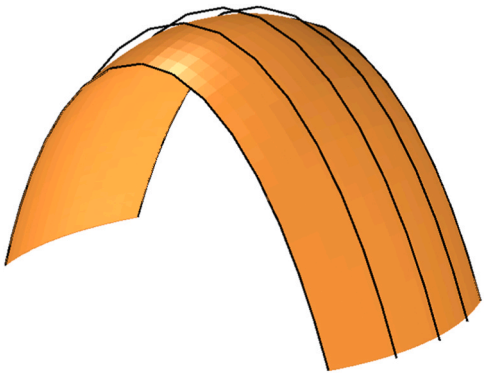

Fig. 2. Fitting a loft to the contours of a form-found surface. The curves are the exact contours along the form-found mesh, whilst the surface geometry is the lofted NURBS surface fitted to them. Note that fewer contours have been used for visual clarity.

To generate extrados faces, a tapered extrusion procedure is employed. By calculating the average normal of the neighbouring panels at vertex points, the points are translated along this normal direction up to a defined plane parallel to the panel (see Fig. 3) based on desired thickness. In this way, the panels end up with regular thickness, and wedge shapes which get wider towards the outside of the shell, while the edge faces form outward slanting trapezoids. The warped transversal faces that arise from lofting the interior and exterior faces are fully connected to their neighbours allowing them to bear the weight of the structure through the interfaces, although the degree of warping is limited due to the low level of curvature. Regarding the complexity of the manufacture for these warped faces, the authors have previously developed a low-cost manufacture method for manufacturing the designed panels with these graded surfaces in timber [47]. For this study

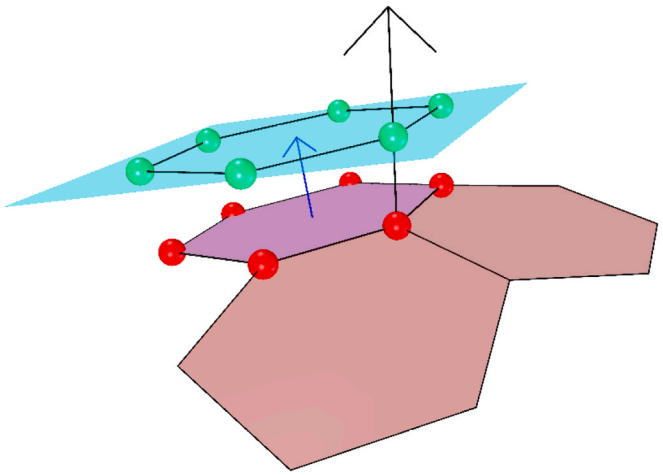

Fig. 3. The tapered extrusion scheme. Taking the base vertex on the right, it is translated along the average normal vector (black) of the three panels displayed which it connects, onto a plane parallel to the panel (given by panel normal, in blue). This leaves the system overlapping slightly at top faces dependent on local curvature, but to a very small order for the panel thickness of 3.6 cm modelled. Loft operations convert the lines to a solid panel. (For interpretation of the references to color in this figure legend, the reader is referred to the web version of this article.).

however, the panels are 3D printed to exactly represent the designed load-bearing surfaces. The regular planar thickness however makes manufacture and assembly easier, whilst the tapered shape is designed to prevent sliding mode failure for the fully assembled structure, as the wedge geometry constrains inward motion by panels. The procedure relies on the use of positive curvature, as the external panel edges will diverge allowing it to work for any thickness. In the case of zero local curvature, the normal directions are perpendicular to the intrados creating a sliding mode, and for negative Gaussian curvature, the normal directions would converge to a focal point creating a thickness limit. Alternative joint styles would be required to kinematically constrain locally negative curvature regions.

The overall effect of the rationalisation into a planar panelled structure has a limited effect on the design envelope, and it may be noted that the structure shown in Fig. 1e bears more resemblance to Fig. 1b than 1d. The tessellation and planarization procedure is the largest source of step-to-step change within the shell geometry, and causes the panels to find a shape which more closely resembled the semi-spherical base design due to the nonlinear interaction of edge length and planarity goals. However, the planarization visually appears to counteract the form-finding procedure. Further work could be developed to combine the form-finding and planarization, to better link the design goals in a single optimisation stage. The structural effect of this planarization will be inspected more closely in Sections 3.3 and 4.1, demonstrating that the joints work to maintain stability despite this shift away from the funicular form.

3.2. Joints design

The goal of the design was to ensure a locally stable structure, that is, one that could stand unaided during the assembly process. From some standard woodworking joint styles, dovetails and finger joints were identified as being potentially viable and manufacturable using digital fabrication techniques.

3.2.1. Parameterisation of base joints

Basic parameterisations of both joint styles were initially created (see Fig. 4). Joints were defined as planar curves to be extruded through mated panels, with a base line of the curve being drawn between coordinates $(0,0)$ and $(1,0)$ in the XY plane. Due to the use of the curves for extrusion, they were closed to allow boundary surfaces to be created. By allowing for the adjustment of the joint parameters, it would be possible to make comparisons between different percentages of edges covered by joints, as well as estimate their effect on deflection properties. For this work, the dovetail parameters were set as $w = 0.3, \theta = 70°$, whilst the finger joints parameters were set as $w = 0.2,\ h = 0.12$.

3.2.2. Calculating panel liaison matrix

To reorient the scaled joints appropriately throughout the structure, it was required to find the topology of the shell structure. In the authors' previous work on shell assembly sequencing [39], the use of scripting was demonstrated for iteratively searching to deconstruct a list of BREPs into their respective faces and find neighbouring faces within a certain tolerance. Using this approach, it is possible to compactly describe the connections in an n-panelled structure as an $n \times n$ liaison matrix.

Taking the topology of a structure of n panels, and labelling the rows and columns as $i, j \in 0 \ldots n$, each item in the matrix for the traditional binary liaison matrix encodes whether there is an edge, i.e. a neighbouring face between two panels as a 1 or a 0 [38]. Some distinction should be made, in that the term liaison matrix is used to describe "liaisons" or interactions between 3D panels at their edge faces, which would generally be described as a face adjacency matrix in 2D meshes. For the current research study, the liaison matrix was extended by additionally comparing panel centroids, and altering the matrix such that neighbours were assigned a $+1$ or -1 depending on whether they are higher or lower than the test panel with reference to the base (Fig. 5). For less regular structures, for example of anticlastic or variable curvature, it might be more appropriate to measure distance in terms of distance in panels from the base, or in some other way consider panel precedence. The modified liaison matrix now additionally encodes

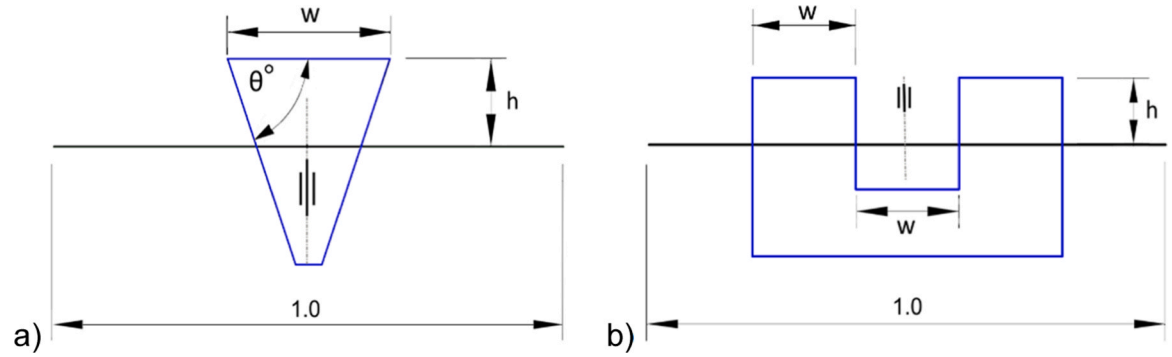

Fig. 4. Parameterisation of the two investigated joint styles, in blue, with vertical lines of symmetry. The reference line in black has length set as 1.0x the length of the edge it will be oriented onto; the w and h parameters are a percentage of this base length. (For interpretation of the references to color in this figure legend, the reader is referred to the web version of this article.)

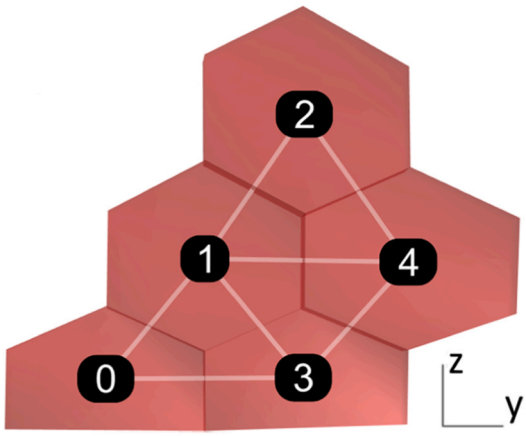

$$L = \begin{bmatrix} 0 & 1 & 0 & 0.5 & 0 \\ -1 & 0 & 1 & -1 & 0.5 \\ 0 & -1 & 0 & 0 & -1 \\ 0.5 & 1 & 0 & 0 & 1 \\ 0 & 0.5 & 1 & -1 & 0 \end{bmatrix}$$

Fig. 5. An example hexagon panel assembly with the liaison graph overlay and associated extended liaison matrix. Note that the matrix could be made antisymmetric by encoding horizontal neighbours as +ve or -ve depending on a relative horizontal location given a selected UV axis, in this case the y-axis shown.

precedence relationships in the structure. In addition, horizontal neighbours could have different joint styles to vertical neighbours to provide changing stiffness along principal stress directions. Horizontal neighbours are shown encoded as values of 0.5, which could be made positive or negative with relation to a selected horizontal axis (y-axis in Fig. 5) to allow for separate treatment of horizontal neighbours. The implementation is provided by iteratively testing the faces within the structure for adjacency; whilst not necessarily the most efficient method for gaining the structures topology, the face boundaries of interface surfaces between panels can be found simultaneously, reducing further computing overhead for modifying the joint edges.

3.2.3. *Propagating joint designs*

Jiménez described the use of such liaison matrices for understanding precedence constraints in assembly sequencing [38]. Now they were applied both for understanding precedence in the assembly and as a tool for deciding where to place sets of joints. Provided the face boundary structure and using Rezaei Rad's exploitation of rigid transformations [48], the previously designed joints in the world XY plane can be reoriented throughout the structure along neighbouring panel's edges.

The parameterised joint curves were scaled to match the length of each top edge, before being reoriented into the plane of the "male" part that will be inserted into its neighbour. Using the liaison matrix, this is decided by propagating male joints only to neighbours with relationships described by a -1 or 0.5, downwards or across. This ensures that each part is inserted male into female from above, implicitly enforcing the precedence requirement that parts are only inserted once all lower neighbours are present.

Once the curves were propagated through the panel edges, they were then converted into planar surfaces and extruded through the thickness of the panel. To enable addition of joint tolerance, scaled copies of each joint were made about centroids, with a scaling factor of $C_{joint} \geq 1.0$, where $C_{joint} = 1.0$ represents a perfect fit and increasing values give greater flexibility in the joint insertion. $C_{joint} = 1.07$ was used throughout.

The extrusion direction for the joints is along the panel normal vectors as described in section 3.1, meaning that the male surfaces end up being perpendicular to the panel face whilst the sliding mode failure of the structure is prevented by the graded edge interface (see Fig. 6). By taking solid Boolean unions of panels with reoriented joint solids, and solid Boolean differences of the neighbour panels with the scaled cutting solids, the panels and their integral joints are generated (Fig. 7). The panels are then able to be fitted via translation into multiple neighbours simultaneously once all neighbouring female slots are located. As noted, this use of the edge faces should constrain panels to prevent inward sliding mode failure, where at least on edge has positive curvature towards the outside of the structure, i.e. in the positive synclastic or anticlastic case. In regions of negative synclastic curvature, alternative joints would be necessary.

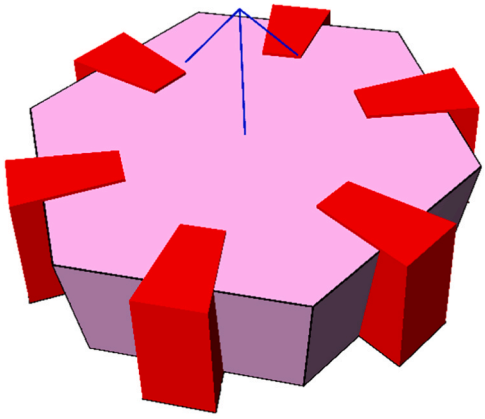

Fig. 6. Central panel in the structure with all male joints. The dovetail wedges are extruded along the normal vector (arrow, blue) of the major panel surfaces; the tapered extrusion of the panel edges themselves prevents sliding modes. Note that the thickness of the panel is exaggerated for visual clarity. (For interpretation of the references to color in this figure legend, the reader is referred to the web version of this article.)

3.3. *Numerical analysis through R-Funicularity*

The relaxed funicularity approach was used to assess the closeness of shell designs to a fully funicular, compression dominated structure. By quantifying the funicularity, and by estimating the effect of the joints on the structure's tensile capacity, the designed structure will be shown to be stable despite issues with the high bending moments due to the planarization. The method will be outlined here and demonstrated on the original, continuous shell prior to planarization, whilst in Section 4.1, the funicularity will also be assessed for the final segmented structure, taking into account the effects of the joints on the structure. The relaxed funicularity (or R-funicularity) method works on the basis that fully funicular forms are free of bending moments, which is highly beneficial for globally stable shell designs. In this work, the method was selected to quantify the funicularity of the shell, examining regions "generalised eccentricity". R-funicularity combines the resultant bending moments and normal forces within the designed fully-assembled shell as a scalar field, as a post-processing technique based on finite element analysis. This field simply demonstrates proportions of

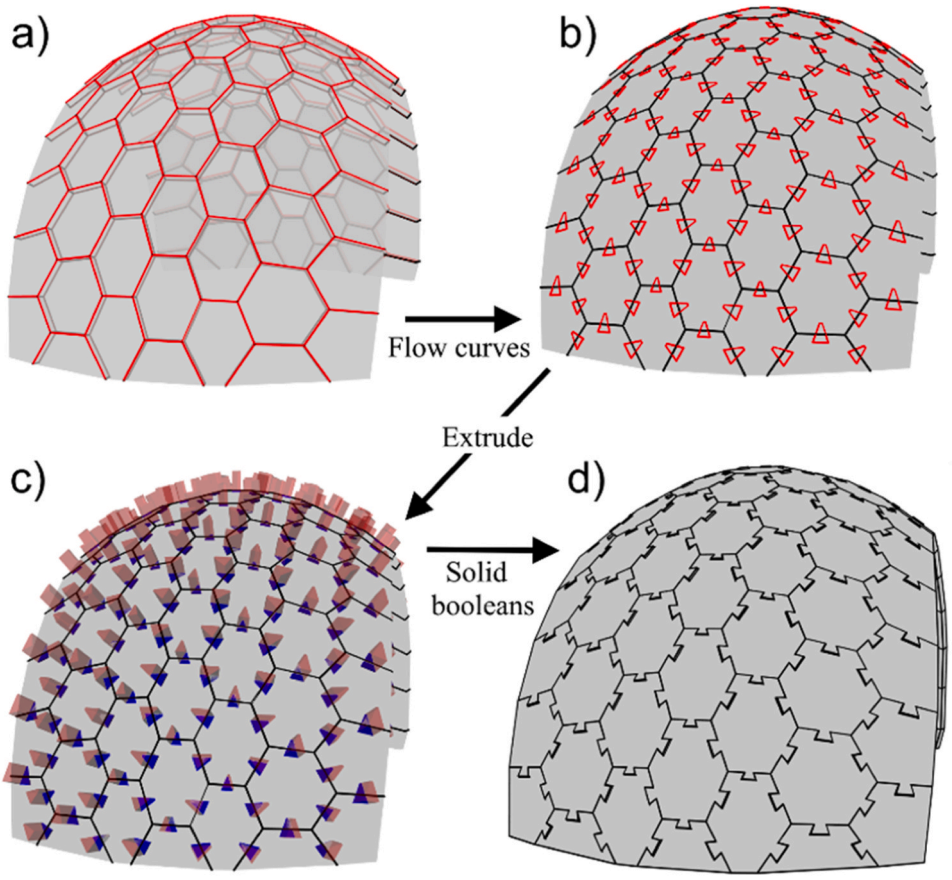

Fig. 7. Flowing and extruding joint curves through the shell geometry. First, **a)** top edges are found, **b)** joint designs are scaled and rotated to match male panel planes, **c)** the curves are extruded with longer, larger red volumes indicating cutting solids, blue indicating joints to union, **d)** final shell. (For interpretation of the references to color in this figure legend, the reader is referred to the web version of this article.)

bending moment stress to normal stress, showing regions that are more prone to separation or require external support. They are used here to give quick visual description of stress conditions through the shell, aiming to show the funicularity at a glance.

By taking the definition of funicularity, that is having purely in-plane membrane forces and zero out-of-plane bending forces, Gabriele et. al proposed a criteria to assess the proximity to a funicular solution [16]. The method is briefly summarised here. Defining the local membrane and bending forces acting at a point on a shell as N_{ij} and M_{ij} respectively, where $i, j \in 1, 2$ representing two local orthonormal axes and $N_{12} = N_{21}$ represents the transverse shear force. Through eigendecomposition of the force formulations, defining a direction angle in the local plane of α where $\alpha \in [0, 2\pi]$, the normal force and bending moment acting along a direction can be expressed as:

$$\begin{pmatrix} N(\alpha) \\ M(\alpha) \end{pmatrix} = \begin{pmatrix} \overline{N} \\ \overline{M} \end{pmatrix} + \begin{pmatrix} \widehat{N} & N_{12} \\ \widehat{M} & M_{12} \end{pmatrix} \begin{pmatrix} \cos(\alpha) \\ \sin(\alpha) \end{pmatrix} \tag{1}$$

where $\overline{N} = \frac{N_{11}+N_{22}}{2}$, $\overline{M} = \frac{M_{11}+M_{22}}{2}$, $\widehat{N} = \frac{N_{11}-N_{22}}{2}$ and $\widehat{M} = \frac{M_{11}-M_{22}}{2}$.

Generalised eccentricity is defined as the ratio of bending to normal forces at a particular location, $e(\alpha) = M(\alpha)/N(\alpha)$. By sampling the eccentricity through a shell and comparing it to an admissibility interval $[-h/6, h/6]$ where h is the thickness of the shell, the shell meets the middle-third criterion if the eccentricity is everywhere within this bound. A recent addition in the topic [49] suggests the modification of the normal force matrix to account for the tensile limit force N_t, making the adjusted eccentricity $e_t(\alpha) = M(\alpha)/(N(\alpha) - N_t)$. The tensile limit force is estimated using an empirical formula for wooden dovetail joints [50] as $N_t = 474N$, based on the smallest panel edge length of 145 mm, thickness of 36 mm and using joint parameters described in section 3.2.

In order to quantify how close the sections are to the relaxed funicularity criteria, the principle eccentricities are taken to be e_1 and e_2 calculated by eigendecomposition [16], and the principle eccentricity with the largest magnitude selected as shown in Eq. (2):

$$e_{absmax} = \underset{x \in \{e_1, e_2\}}{argmax}(|x|) \tag{2}$$

For comparison with the eccentricity bounds $[-\lambda h, \lambda h]$, where λ is the eccentricity limit, the maximum absolute value of the principal eccentricities is normalised as:

$$F_{funic} = 1 + \frac{e_{absmax} - \lambda h}{\lambda h} \tag{3}$$

Note that through this conversion to a normalised eccentricity factor using a value of $\lambda = 1/6$, F_{funic} values $0 \leq F_{funic} \leq 1$ indicate a region which fully meets the relaxed funicularity middle third criterion ($\lambda = 1/6$), whilst values $0 \leq F_{funic} \leq 3$ indicate those where the bending force lies within the material thickness (Fig. 9).

This formulation provides a graphical representation of the forces and funicularity through the shell. Fig. 9a demonstrates regions (in blue) of potential concern where the bending moments are significant, and comparison to the FEA results of Fig. 8 show that these points correlate well to the tension in the shell. Fig. 7.b demonstrates how these regions act; pink regions are those where the shell transitions between tension and compression, indicating where additionally the bending moment changes direction. The analysis based on the adjusted eccentricity predicts a fully R-funicular shell..

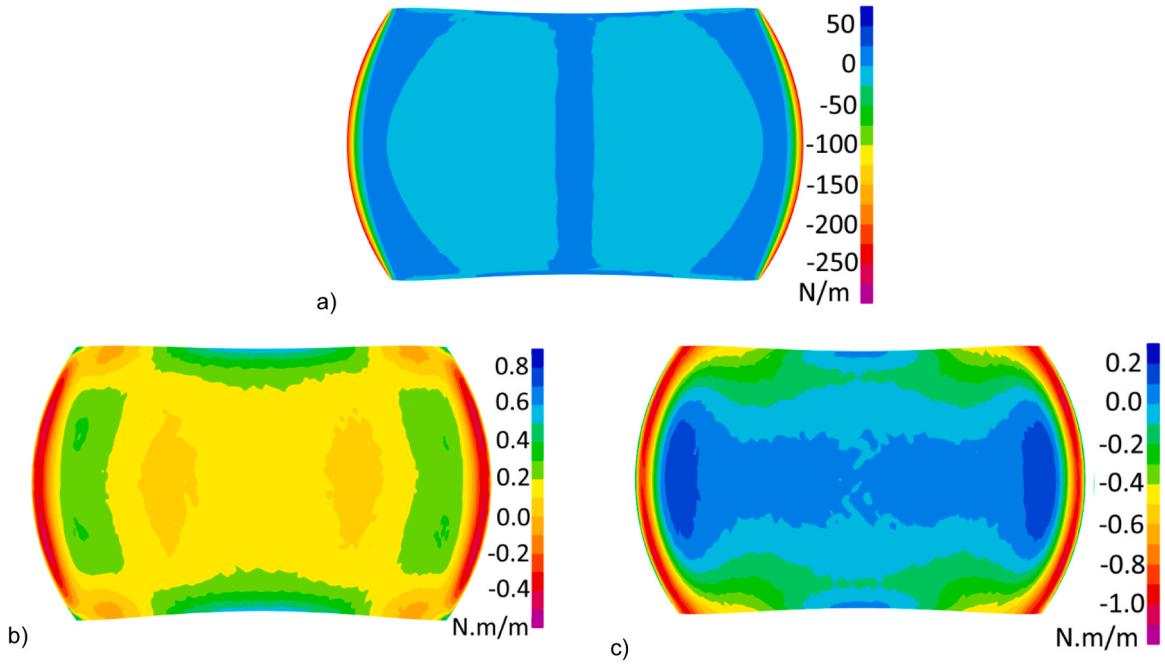

Fig. 8. FEA results for the initial shell form-found in Grasshopper. **a)** F_{MAX} values through the shell in N/m. Note that the darker blue region indicates a small amount of tension, up to 25 N/m. **b)** M_{MAX} values through the shell thickness in Nm/m. **c)** M_{MIN} values through the shell thickness in Nm/m. (For interpretation of the references to color in this figure legend, the reader is referred to the web version of this article.)

3.4. Stability assessment through coupled rigid-block analysis (CRA)

Whilst the R-funicularity approach is useful for determining the funicularity and suitability of a fully assembled shell to support itself through compression, it is not designed for discretised structures. The setting up of FEA models for segmented integrally joined shells is complex owing to modelling all possible interactions. The coupled rigid-block analysis is an optimisation based approach used to assess the stability of an assembly comprising of rigid blocks [51]. The analysis was implemented via the Python package COMPAS CRA [52] within the design software for the purpose of assessing stability of the designed structure, not only when fully assembled but also throughout the assembly process.

To validate the CRA analysis for such discretised shells, a subsection of the full shell was selected for manufacture. Testing was done by comparison of CRA to measurements of the deflected height for the central 3D printed panels.

By adding a small change to the code for COMPAS CRA to describe extra loads in [53], it can also allow the addition of external forces to the model and thus estimate the effects of additional dead loads on the structure. The models are exported to Python using JSON data, which were analysed for stability and displacement at various steps through the assembly process before being passed back to CAD for inspection.

3.5. Infinitesimal blocking relationships and inter-panel constraint assessment

Assembly sequencing allows a different insight into the assembly, allowing us to find a) if it is possible to assemble the arch using translational movements, and b) a sequence of parts and insertion directions. This research study focuses on the former objective. Previous work [39] detailed the implementation of this process and the software components created towards assembly sequencing, and the aspects relating to inter-panel constraints are briefly touched upon here.

The general procedure is shown in Fig. 10 working on a single interface, although for calculation the spheres of blocking directions are discretised into a test set of possible vectors, distributed evenly. The normal directions of all the planes comprising an interface surface, for panel i from neighbour j (with neighbours given by the previously generated liaison matrix), can be collected into a set, $X_{normal.i.j}$. Additionally, a set of test vectors of unit length, X_{test}, is generated, evenly sampling 3D space through a Fibonacci sphere. By comparing every interface vector with every test vector, the condition for a direction that the panel motion is blocked translationally by a neighbour is:

$$\vec{x}_{test} \cdot \vec{x}_{normal} > 0 \tag{4}$$

and these matching vectors are added to a set $X_{\text{blocked i,j}}$, whilst free directions are the set difference of test vectors and blocked vectors,

$$X_{freei.j} = X_{test} \setminus X_{blockedi.j}. \tag{5}$$

As panels are added to the structure, further neighbours block motion of parts, increasing the number of constrained translational directions for each panel:

$$X_{free \cdot i,Total} = X_{free \cdot i,ngbr1} \cap X_{free \cdot i,ngbr2} \cap \ldots \cap X_{free \cdot i,ngbrN} \tag{6}$$

where $X_{free \cdot \text{i,Total}}$ is the total set of free directions for element i and $X_{free \cdot \text{i,ngbrN}}$ is the set of free directions of element i with respect to a particular liaison. The number of test vector directions which are blocked, or conversely, the number of free test vector directions, quantify the level of part constraint or freedom, which can thus be assessed based purely on the geometry of part-part interfaces and neighbour topology of the structure. It is possible that a panel has no free insertion directions, that is, for panel i the set $X_{free \cdot i,Total}$ is empty. In this case, an alternative assembly sequence should be sought with alternative preceding neighbours, or if this is not possible, the design is infeasible and should be reconsidered [39].

4. Results

4.1. Funicularity of the final design

The shell was analysed using FEA software SAP2000 for the segmented case, with pinned based nodes and gravity applied

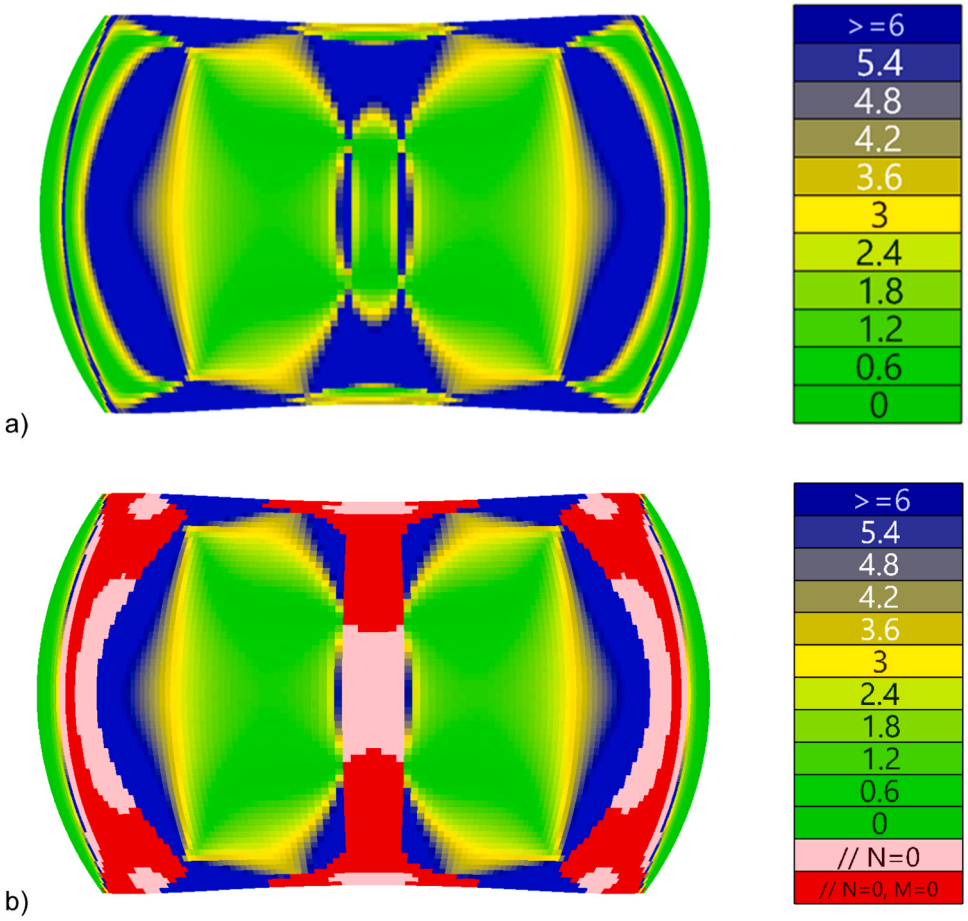

Fig. 9. a) Proposed graphical representation of the R-funicularity, showing values of F_{funic}. For this form-found shell of thickness 3.6 cm and span 1.6 m, 85.5 % meets the middle third criterion while 94.5 % is within the shell thickness. Figures are dimensionless. **b)** highlights areas where the force axis, or both the force and moment axis are crossed, such that the region is either changing from tension into compression (pink), or additionally regions of contraflexure, where there is also a predicted change in sign of bending moment (red). (For interpretation of the references to color in this figure legend, the reader is referred to the web version of this article.)

throughout to test static dead loading capability. A timber material was modelled of density $600 kg/m^3$, modulus of elasticity 13.7 GPa, Poisson's ratio 0.4. By exporting the FEA results to CSV files, the intermediate steps could be assessed using the R-funicularity approach within a user friendly CAD environment, to examine the necessary design steps approach or diverge from an "ideal" funicular shell. For the panellised shell described, the panels are joined into a single kinked mesh surface comprising of a set of thin shell analysis elements (Fig. 11). A linear elastic analysis is used, with the base points constrained by pin supports. The use of a single continuous mesh is justified by the assumption that the panels remain locked for the assembled shell, such that normal forces are transferred through the panel edges.

From Fig. 12a, which shows the maximum normal forces on the shell elements, it can be seen that the majority of the 3.6 cm thick shell exhibits compressive (negative) force, with some tensile regions appearing in a band towards the base signified by the lighter region. This suggests a potential failure area for the shell approaching the base.

In Fig. 12b, which views the bending moments on the shell elements, high positive bending moment regions are exhibited at the central free edges of the structure, as well as a small section towards the edges at the base. This suggests possible regions of non-funicularity, which could be mitigated by using edge supports. Without panel joints the regions at the edges would likely be a collapse area due to loss of panel cohesion. Large negative bending moments are also shown on the angular regions at panel edges, suggesting that the structure is held stable by shared panel edges where joints lie.

Taking the normal force and bending moment force tensors, the R-funicularity of the structure was analysed at each element using Eq. (1), and normalised to check how close the structure is compared with an ideal R-funicular shell.

Fig. 13 shows a graphical representation of the eccentricity of the shell using the normalised eccentricity from (3). The shell is provided with a material thickness of 3.6 cm and has a max span 1.59 m, while the material is selected as Birch ($E = 13.7 GPa$, Poisson's ratio $\nu = 0.4$). By counting the discretised mesh faces that meet design criteria, 55.9 % of the planarized shell meets the middle third criterion and can be thus considered R-funicular, whilst 79.5 % of the shell meets the $\lambda = 1/2$ criteria. Halving the thickness to 1.8 cm, 70.9 % meets the middle third RF criterion, whilst 87.8 % meets the $\lambda = 1/2$ criterion. Fig. 14 shows the eccentricity ranges for the regions highlighted in Fig. 13. In Fig. 14b, the effective tensile force formulation is applied on the 3.6 cm thick shell, having the effect of shifting the graph to the left. Note that using the effective eccentricity, the entire shell is R-funicular within the $0 \leq F_{funic} \leq 1$ admissibility range.

4.2. Initial validation of CRA for local assembly stages of a 3D printed shell subsection

The entire rigid block assembly was incorporated into the CRA solver initially to verify the stability of the structure. A material density of 1.25 g/cm^3 is used, with a PLA-PLA friction coefficient of 0.3824 [54]. The solver predicted that the structure would be fully stable once assembled,

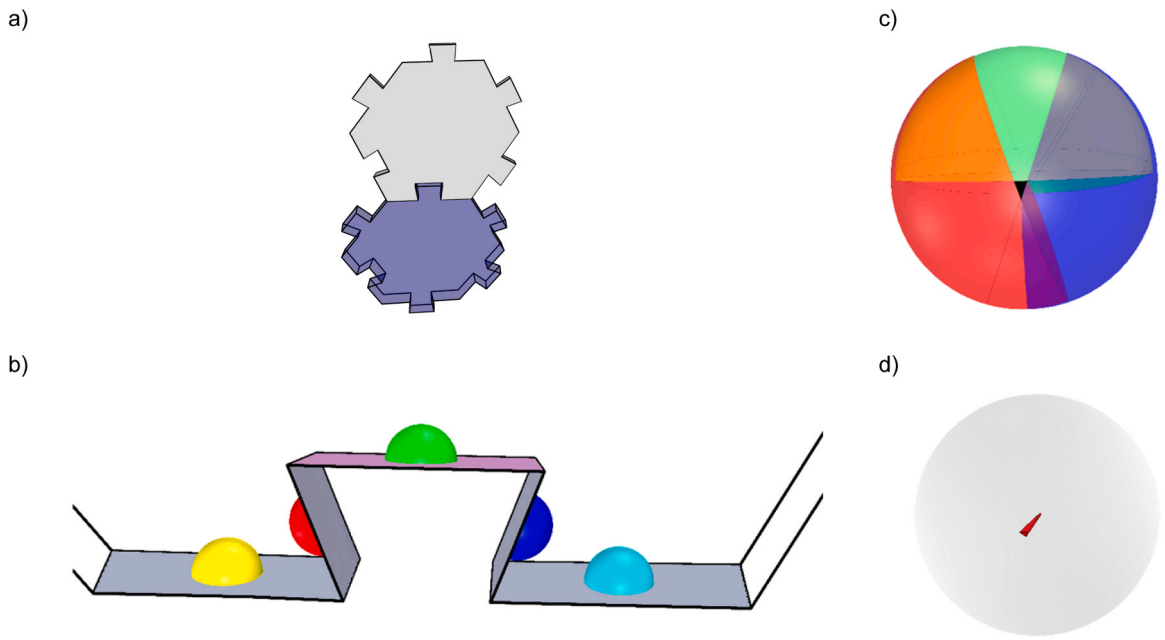

Fig. 10. The blocking directions acting along a single panel interface. **a)** The panel in the structure being inspected (white) with the panel for insertion (blue). **b)** The directions which each face of the interface blocks for the neighbours translational movement are shown, on a panel viewed from above. **c)** The union of the blocking directions viewed from above. The blocking directions leave a small section of the sphere shown in black, which is unblocked – this is the set difference of all possible directions and the union of blocked directions. **d)** The small remaining set of vectors with translational freedom for this interface are highlighted, from the side. This shows the possible insertion vectors for the neighbouring panel. (For interpretation of the references to color in this figure legend, the reader is referred to the web version of this article.)

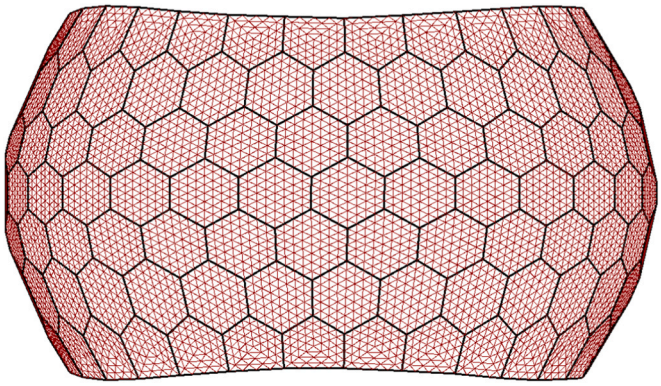

Fig. 11. Structure discretisation scheme in red, tile edges in black. The discretisation is generated by connecting vertices of panels to the geometric centres, giving 5–6 elements per panel for this hex-dominant tiling, before refining the mesh. This maintains the sharp edges between panels for FEA.

despite the non-funicular regions predicted by the R-funicularity analysis. A 3D printed model of an arch section was then created, with the CRA analysis run on the same set of panels for comparison. By removing segments of the fully assembled arch in both the analysis and the physical model, the suitability of CRA for the assessment of the dovetail joint design at maintaining stability during assembly could be verified..

Going through the assembly steps for the 3D printed arch model depicted in Fig. 15b, the structure was predicted by CRA to be stable during the intermediate assembly stages. Assessment is made by removing panels from the full arch and comparing to the same CRA model – referring to Fig. 15b, test case 1 requires removing the central member (labelled 1); case 2 requires additionally removing the two panels either side (labelled 2), and so on. The stability relies on the friction between joints to counter the cantilevering effect on the structure, and the physical model assembled by hand matched these predictions (Fig. 16). The deflected heights at the furthest extent were measured and compared to predictions from CRA.

In Table 1, there is significant deflection in the structure, which is most noticeable at case 1, with a maximum drop of 28% at the end point and least visible for the parts closest to the base. A relatively small sag is exhibited in the fully assembled arch, as would be expected since the arch has support from both ends and is based on a funicular form.

The modified CRA Python script with added loads was tested against the assembled arch model by gradually increasing vertically downward dead loads on the top central panel, first in 10*g* increments and then a 1*g* search space once the failure region was found, ultimately predicting a max load of 823 g; the arch spanned 510 mm with a max height of 250 mm and panel thickness 5 mm. A further R-funicularity analysis was also made on this same subsection of shell, for comparison (Fig. 17). The assembly was tested physically using a 3D printed prototype, and the structure successfully supported a 590 g measuring tape (Fig. 18). It should be noted that it was precarious and seemed unlikely to accept any more mass, as the panels were shifting and pushing outwards towards the base. Another R-funicularity analysis with a conservative tensile limit force of 20 N was run for direct comparison with this loaded state, and the failure of the arch aligned with the two regions noted as blue in Fig. 17, around 3 panels up on the R-funicularity plot where the shell is non-funicular. This failure is predictable for the form as it has not been specifically designed with this external force in mind, and the failure region highlighted by Fig. 17 is commonly indicated as a maximum bending moment region in arches [55]. The actual loading capacity is lower than that predicted by the analysis; the conclusion is that this is due to the manufactured PLA model having a lower coefficient of friction than estimated from previous research, due to manufacturing tolerances in the joints.

4.3. Comparison of joint styles

Applying the same CRA case study to a finger jointed version of the structure, whilst the fully assembled arch was found to be stable as

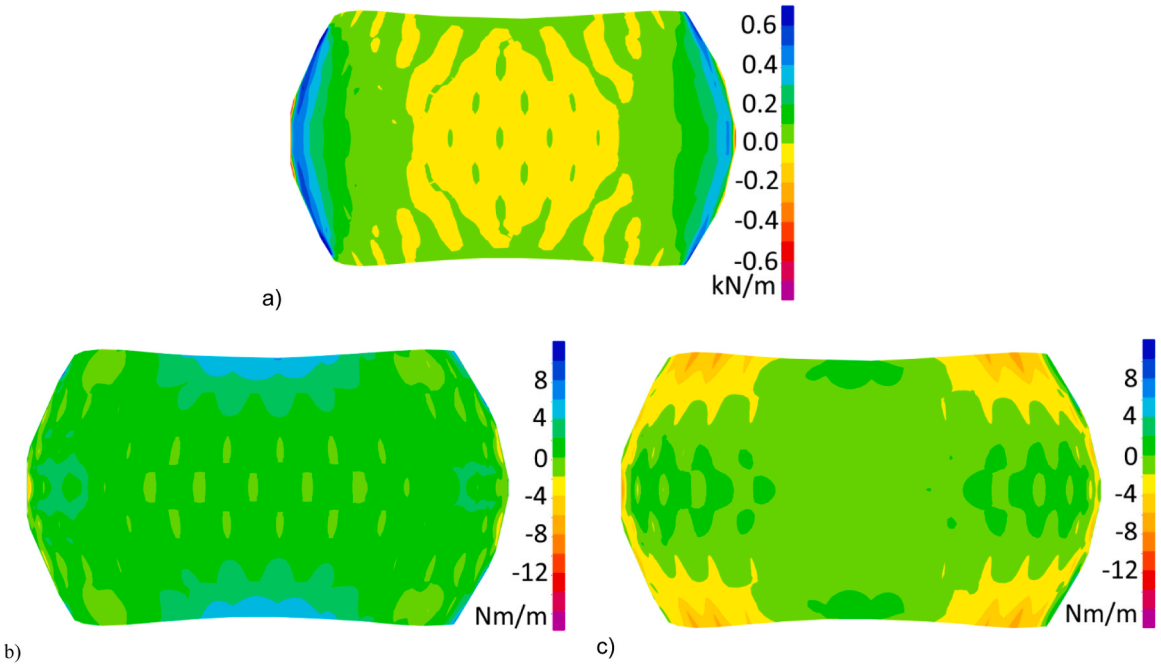

Fig. 12. FEA results for the planarized hex-dominant shell. **a)** F_{MAX} values through the shell in kN/m. The yellow region is fully in compression. **b)** M_{MAX} values through the shell thickness in Nm/m. **c)** M_{MIN} values through the shell thickness in Nm/m. (For interpretation of the references to color in this figure legend, the reader is referred to the web version of this article.)

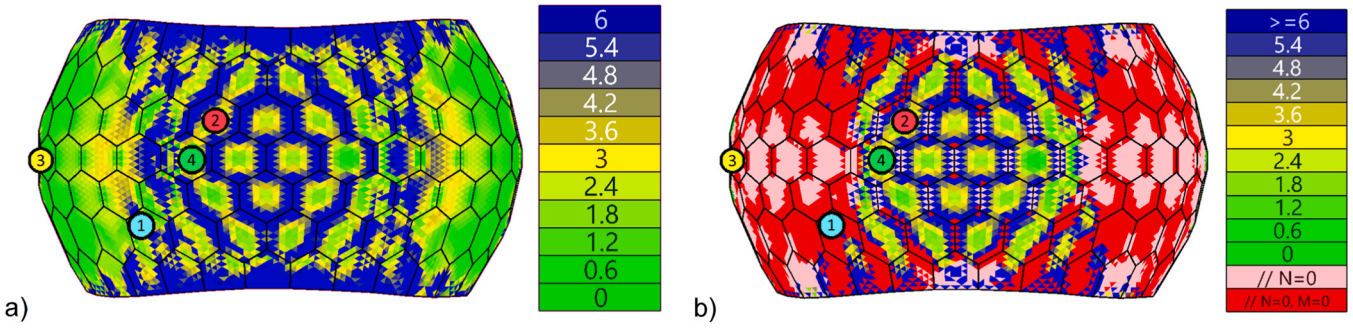

Fig. 13. R-funicularity analyses for the hexagonal shell. Green areas close to meeting the middle-third criterion (<1/6), yellow being within the material thickness (<1/2). Highlighted are some points for inspection. **a)** shows the normalised funicularity values. **b)** highlights areas where the force axis, or both the force and moment axis are crossed, such that the region is either changing from tension into compression (pink), or additionally regions of contraflexure, where there is also a predicted change in sign of bending moment (red). (For interpretation of the references to color in this figure legend, the reader is referred to the web version of this article.)

expected due to its funicular nature, only cases 4 and 5 (see Fig. 15b) were predicted stable from the set of reduced arches, with the mass of panels in longer cantilevered assemblies causing rotation about the joint interface and failure.

Inter-panel constraint assessment also provided some differing results between the two joint styles (Fig. 20). The dovetail style is kinematically self-constraining, such that at any time, only the uppermost members without higher neighbours can be removed. Comparatively for the finger-jointed structure, there is more freedom within the structure at any time – large areas of panels could be removed at once, as the panels are not blocked translationally by their higher neighbours. This means that panels could also be removed from the middle of a structure, which while it may be of some benefit to assembly, would increase risk for sliding mode failure.

Interestingly, the inter-panel constraints are noted in this case study to complement the conclusions of the CRA analysis. While a fully constrained set of panels as described by Fig. 20a are not necessarily a precursor to a feasible assembly, they do seem to increase the likelihood of local stability.

5. Discussion & conclusions

The approach outlined for generating shell forms shows benefits in the use of an extrusion regime for the panel and joint vertices. Varying extrusion vectors prevents sliding failure of structures through dead gravity load; this is corroborated by the CRA and model results for the partial structures, where cantilever effects are allowed by the constraints imposed through the wedge-shaped extrusions. In generating the shell, the conversion from meshes back to a single untrimmed NURBS surface using mesh contours is a minor contribution, necessary to make use of most panelling tools which project hexagons using UV parameterisation. This conversion is however only suitable for a small subset of shells, namely arches or extruded catenaries where the majority of the shell runs parallel to a single longitudinal axis, and other explorations in literature exist which apply in more general cases. Alternative techniques for tiling the more general shell should be explored, which are

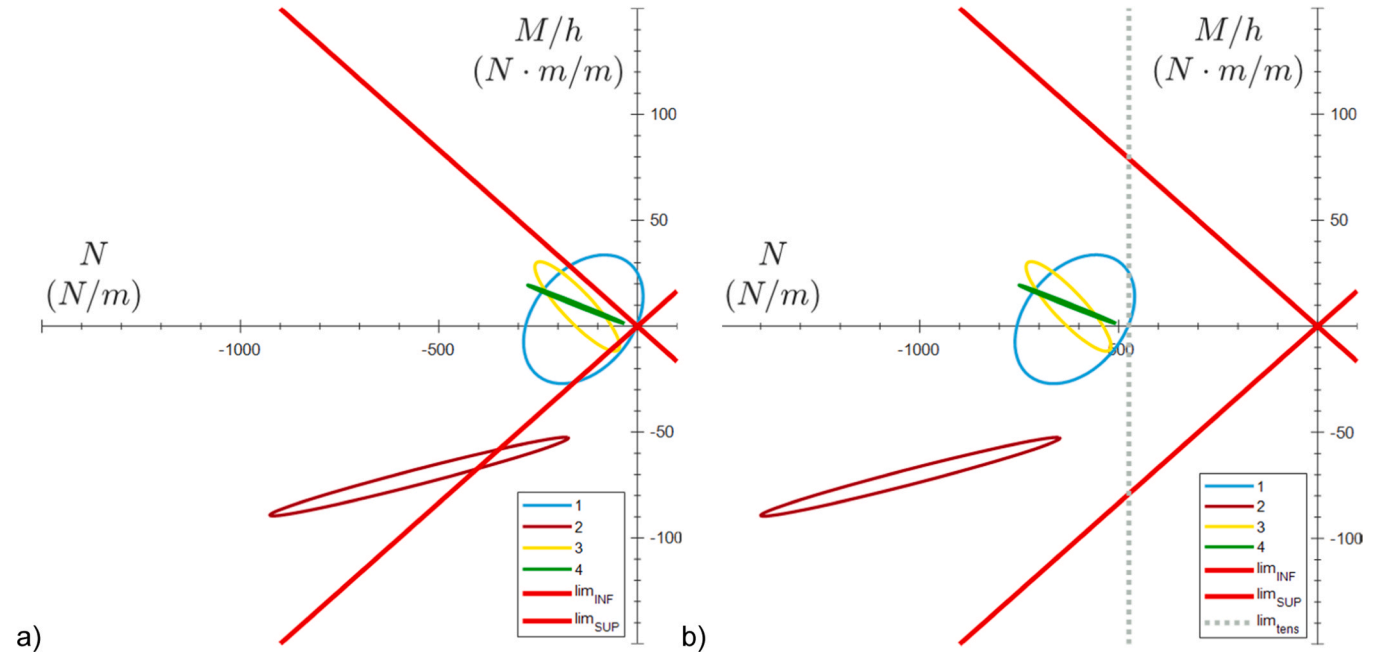

Fig. 14. a) Bending moment (divided by shell thickness) against normal force, demonstrating the eccentricity of the points in Fig. 13 in all directions. **b)** The effective eccentricity graph, using a tensile limit force $N_T = 474N$. The dashed line shows the shift that the tensile limit force imparts in the X-direction.

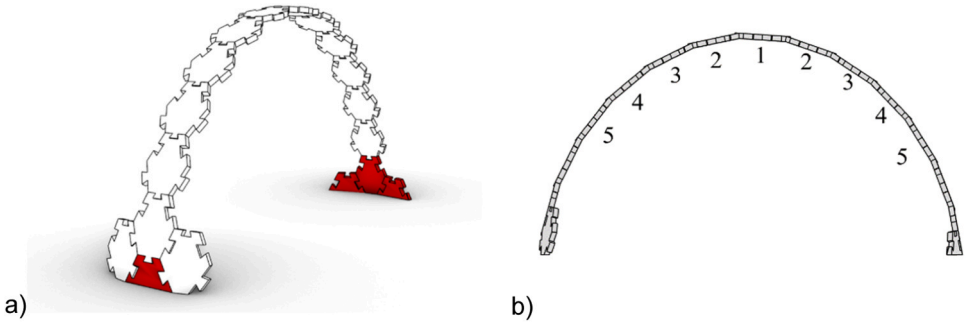

Fig. 15. a) Subset of panels from the full shell in Fig. 11 tested via CRA and through 3D printing. Red panels are those set as fixed base points for CRA modelling. **b)** Numbered sequence of panels removed during the test. Number labels denote that these panels, and those of lower numbers are removed for this case number. Case 0 is the fully assembled arch.

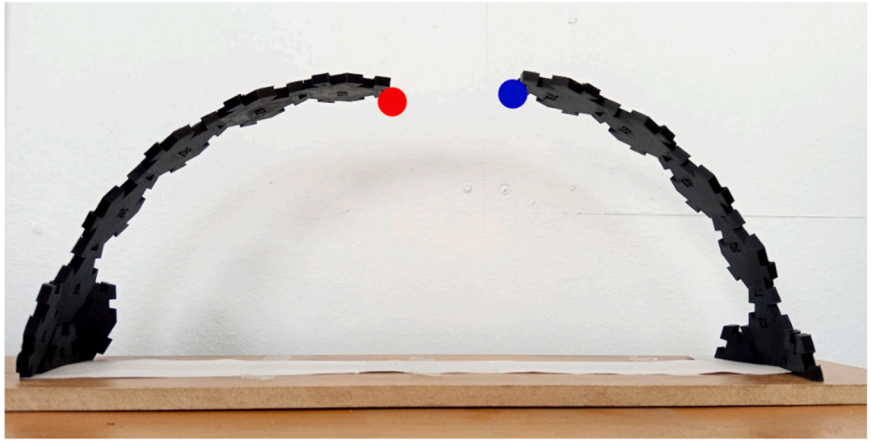

Fig. 16. The partially assembled 3D printed arch with 3 central panels removed (case #2, see Fig. 15b). Note that the red dot indicates the point at which the left hand height measurement is taken for this case, whilst the blue indicates the right. As predicted, the cantilever is self-supporting through the friction and rotational action on joints. (For interpretation of the references to color in this figure legend, the reader is referred to the web version of this article.)

Table 1
Comparison of predicted vs measured deflection heights and prediction error for 3D printed arch vs. CRA model, with cases from Fig. 15b, taking measurements from both left and right free ends.

Case #	Design height (mm) h_d		Predicted height (mm) h_P		Measured height (mm) h_m		Difference (mm) $h_m - h_p$		% Deflection $-\frac{h_m - h_d}{h_d}$		Error (%) $\varepsilon = \frac{h_m - h_p}{h_m}$		Average absolute error (%) $\frac{\lvert\varepsilon_L\rvert + \lvert\varepsilon_R\rvert}{2}$
	L	R	L	R	L	R	L	R	L	R	L	R	
0	250	246	241	239	243	240	2	1	3	2	1	0	1
1	250	246	187	201	179	190	-8	-11	28	23	-4	-6	5
2	239	228	198	201	202	194	4	-7	15	15	2	-4	3
3	213	197	190	183	190	179	0	-4	11	9	0	-2	1
4	178	156	165	150	166	148	1	-2	7	5	1	-1	1
5	133	108	129	108	129	105	0	-3	3	3	0	-3	1

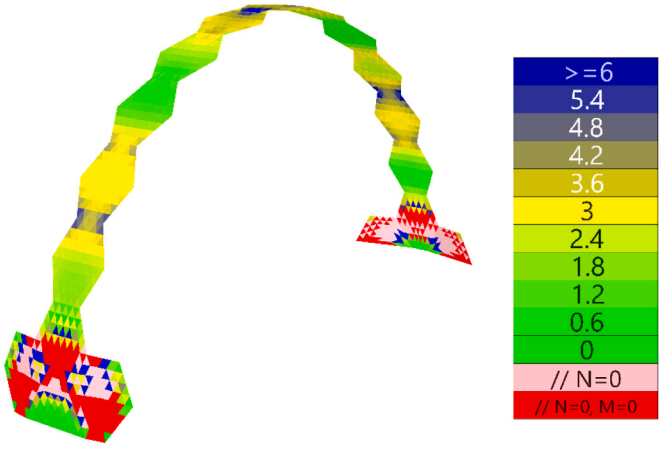

Fig. 17. The R-funicularity analysis for the arch subsection of the shell, using a tensile limit force of $N_t = 20N$.

not so reliant on using UV-parameterised surfaces, and other research is focused on such free-form surface tiling [45], however for cases with 4 edges which can be described as a quadrilateral mesh, the approach described is acceptable.

The proposed joint propagation technique considers the relative sizes of panels by scaling and reorienting a base joint design. The technique also allows for rapid changes to the joint style. It relies on the basis that there is only a single interface edge between panels and would require modification to work also with concave edged tiles. The technique is more generally suited to forms of positive gaussian curvature, although it would be possible to use multiple joint styles applied selectively throughout a structure dependent on local curvature.

The considered R-funicularity approach, and the proposed graphical representation provide a reasonable general overview of the shell forces and funicularity, along with how the different regions act with relation to changes in sign of normal and bending forces. The normalisation of the eccentricity gives a method of generalising the R-funicularity measurement to remove the reliance on shell thickness, allowing for ease of comparison between different designs and presenting information in a useful manner for identification of non-funicular regions; the use on the arch model for example demonstrates a failure region when subjected to a vertical point load. The R-funicularity assessment based on principal eccentricities is not necessarily ideal due to the problems introduced by the changes in sign of forces, and a better approach might be to look at sampling the eccentricities over a range of angles to ensure that they all lie within the eccentricity bounds. Regardless, conclusions can be drawn from the images generated about how the shell will act, where failure areas may occur (as seen in the dead loading of the 3DP structure), and locations which may require additional formwork. Further, the use of the tensile limit force formulation predicts that the joints, which confer tensile strength on the structure by both their shape and through friction, can maintain the R-funicularity of the structure preventing its collapse.

While the R-funicularity approach deals with the fully constructed shell, acting as a useful postprocessing step on the linear elastic FEA analysis, CRA is shown to be a better assessment of stability for discrete structures. CRA here demonstrates how, despite regions of low funicularity, joints can take on the introduced tension and bending moments to maintain structural stability, agreeing with the tensile limit force formulation. Additionally, the technique is shown to predict the stability for intermediate assembly stages, and indeed verifies the feasibility of the dovetail joint style in self-supporting the 3DP arch during construction. Further work should be done to assess the changes in deflection introduced by altering joint parameters, and to understand the increase in error introduced by scaling on the deflection predictions. Possible causes for this worth examining further could include part tolerances along with the virtual displacement calculations provided by CRA. The stability assessment appears sound, although one caveat is that it is a technique designed for rigid blocks such as masonry, and as such, would be less appropriate for more flexible panels over larger scales.

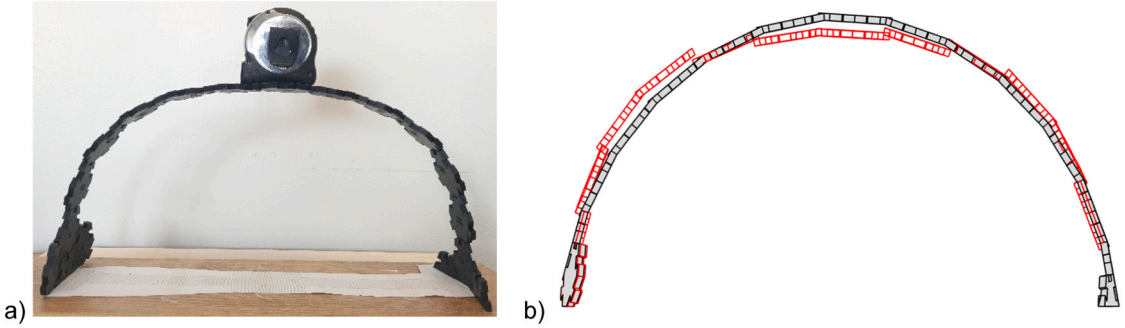

Fig. 18. Dead load testing. **a)** The shape of the structure can be seen with a mass on the central panel. **b)** The CRA model of the structure with its ultimate load, where the panels are predicted to separate (original design in black, failure mode in red). (For interpretation of the references to color in this figure legend, the reader is referred to the web version of this article.)

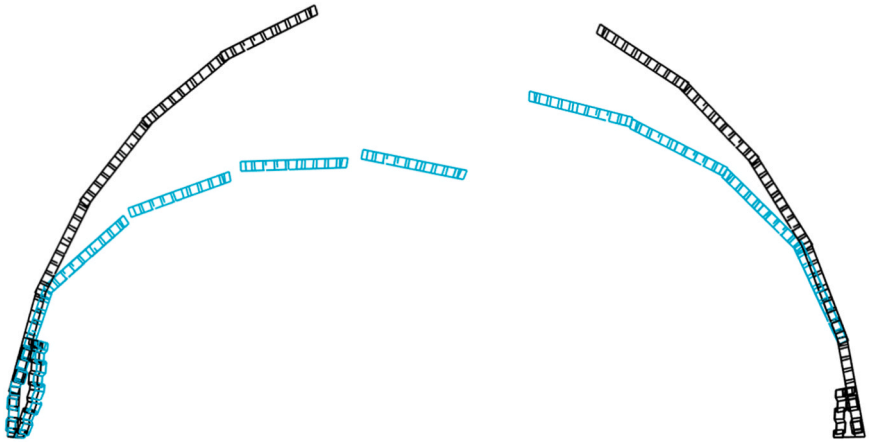

Fig. 19. Predicted failure of the finger jointed design.

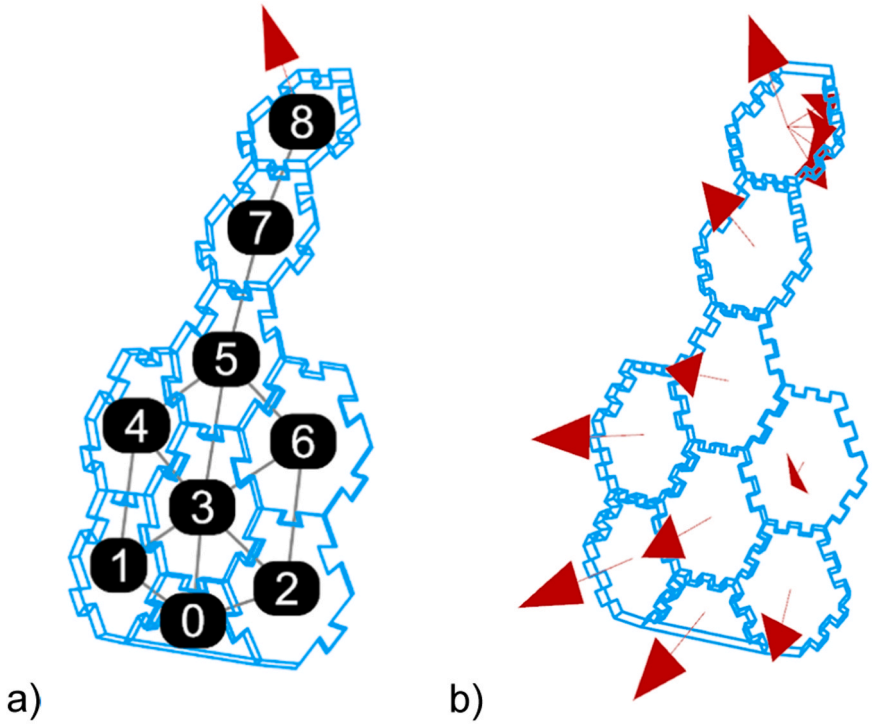

Fig. 20. The results of the assembly sequencing/free direction testing for test structure of 9 panels. **a)** The dovetail joint system has only 1 panel which isn't completely constrained by its neighbours (the top panel #8). **b)** Each finger jointed panel has at least 1 vector of translational freedom, by which the panel can slide causing failure during assembly.

The developed inter-panel constraint assessment gives a visual representation of local part freedom, providing a way of understanding constraints. Additional work could demonstrate, through graph search techniques, the use of these constraints to find feasible assembly sequences, as discussed by other authors [28,38]. The constraints show some correlation with the results of CRA, with finger jointed panels, which have lower levels of inter-panel constraint, being more susceptible to sliding failure and unsuitable for unsupported assembly here.

In comparing the different approaches used, the R-funicularity analysis is based on a linear elastic finite element analysis, using a continuous mesh to approximate the compressive and bending force through the assembled shell. A continuous mesh is justified here by the assumption that the panels have tight enough joints to transfer loads through interface edges. Using coupled rigid block analysis, which works on the non-linear behaviour of friction and contact forces acting between discrete elements, there is shown to be some alignment when comparing to the non-funicular regions arising on the RF plot of the arch subassembly. There are accuracy benefits to using a linear analysis at the large scale, and using a non-linear analysis for the smaller scale, as it is easier to estimate discrete panel behaviour and movement using the discrete analysis. It could be informative to use non-linear FEA analysis of structures and make comparisons, particularly at larger scales where the error induced by using rigid blocks will be higher.

A single case study has been conducted examining a single simple shell design using FEA and rigid body analyses. It has been demonstrated however that the tensile limit force extension of R-funicularity can correctly predict the stability of segmented shells with integral joints, provided the tensile force that joints can confer is calculated. Further design explorations should be made particularly for shells with openings and for a wider range of joint styles. The approach of using a rigid body

mechanics formulation has been shown to correctly predict the stability of the structure at intermediate design stages for this study, relying on cantilevering effects to avoid formwork. This is shown to correlate with R-funicularity results for the provided example. The methodology applied should also be applicable to more free-form designs, where the CRA analysis and the tensile limit force can be used to predict stability caused by integral joints, despite issues with funicularity. The use of the discrete analysis is somewhat limited by elastic effects, and the scale of the structure should be considered when applying to ensure that flexural effects don't invalidate the predictions. Ongoing work could consider the applicability of the proposed approach to also assessing complex geometry curvature, and the capability of the discrete analysis in particular at modelling regions of negative local curvature. Such designs would require careful reconsideration of the joint style to ensure that panels remain kinematically constrained.

The presented integrated approach to the design of discretised shells highlights the combined use of 3 different computational tools, showing their complementary use to provide early-stage design feedback. R-funicularity demonstrates the funicularity and therefore ability to self-support once fully assembled, as well as quantifying the change introduced to a form through different design stages. CRA acts as a predictor for the stability of the structure once discretised into panels with joints, allowing understanding of the stability of intermediate assembly stages; and inter-panel constraint assessment is utilised to display the part insertion vectors allowed between neighbouring parts, highlighting constrained directions in the assembly to compare between panel joint designs and show the implications of joints on the assembly sequence. Using the combination of these tools, designers can access a range of information describing numerous hierarchical degrees of discrete shell structures' stability, ranging from the full shell down to the individual panel. With a 3D printed model, this work has demonstrated that the stability assessment is correct for a certain scale, using no external scaffolding, adhesives or fixtures, as opposed to the previously cited hex-dominant shell designs. Further research will be required to demonstrate the culmination of these works into a full shell demonstrator in timber, to further assess suitability of the combined design approach at structural scales. With integrated analyses, the use of computational tools and design feedback will clearly become increasingly ingrained into current design software, to further blur the lines between architecture and engineering. Such tools for stability analysis and part design can, and hopefully will, lead towards rapid improvements in the speed of realisation and quality of construction for computationally designed, feasibly fabricated architectural structures.

CRediT authorship contribution statement

Sam Wilcock: Conceptualization, Data curation, Formal analysis, Investigation, Methodology, Project administration, Software, Validation, Visualization, Writing – original draft, Writing – review & editing. **Mehmet R. Dogar:** Project administration, Resources, Supervision, Writing – original draft, Writing – review & editing. **Han Fang:** Methodology, Resources, Supervision, Writing – original draft, Writing – review & editing. **Ornella Iuorio:** Conceptualization, Data curation, Formal analysis, Funding acquisition, Investigation, Methodology, Project administration, Resources, Supervision, Validation, Writing – original draft, Writing – review & editing.

Data Access Statement

The data associated with this paper are openly available from the University of Leeds Data Repository. https://doi.org/10.5518/1537

Declaration of Competing Interest

The authors declare that they have no known competing financial interests or personal relationships that could have appeared to influence the work reported in this paper.

Acknowledgements

The authors would like to thank Dr. Antonino Iannuzzo (University of Sannio, IT) for his time and discussions relating to structural stability, and the anonymous reviewers for their comments. This work was supported by the Engineering and Physical Sciences Research Council [EP/T517860/1]. For the purpose of open access, the author has applied a Creative Commons Attribution (CC BY) licence to any author accepted manuscript version arising.

References

[1] Marmo Francesco, Rosati Luciano. Reformulation and extension of the thrust network analysis. Comput Struct 2017;182:104–18. https://doi.org/10.1016/j.compstruc.2016.11.016.
[2] Block Philippe, Dejong Matt, Ochsendorf John. As hangs the flexible line: equilibrium of masonry arches. Nexus Netw J 2006;8(2):13–24. https://doi.org/10.1007/s00004-006-0015-9.
[3] Kai-Uwe Bletzinger, Ramm Ekkehard. Computational form finding and optimization. In: Adriaenssens S, et al., editors. Shell structures for architecture. London, U. K: Routledge; 2014. p. 45–55. https://doi.org/10.4324/9781315849270 (et al.).
[4] Moskaleva Anastasiia, Gusev Sergey, Konev Stepan, Sergeichev Ivan, Safonov Alexander, Hernandez-Montes Enrique. Composite freeform shell structures: design, construction and testing. Compos Struct 2023;306:116603. https://doi.org/10.1016/j.compstruct.2022.116603.
[5] Rutten David. Grasshopper 3D. Robert McNeel and Associates; 2007.
[6] Tang Gabriel. An overview of historical and contemporary concrete shells, their construction and factors in their general disappearance. Int J Space Struct 2015;30(1):1–12. https://doi.org/10.1260/0266-3511.30.1.1.
[7] Bertetto Amedeo Manuello, Riberi Federico. Form-finding of pierced vaults and digital fabrication of scaled prototype. Curved Layer Struct 2021;8(1):210–24. https://doi.org/10.1515/cls-2021-0020.
[8] Rippmann Matthias, Block Philippe. New design and fabrication methods for freeform stone vaults based on ruled surfaces. Springer Berlin Heidelberg,; 2011. p. 181–9. https://doi.org/10.1007/978-3-642-23435-4_21.
[9] Mele Tom Van, Popescu Mariana, Augustynowicz Edyta, Echenagucia Tomsas Mendez. The Armadillo vault computational design and digital fabrication of a freeform stone shell. Advances in architectural geometry 2016. Zurich, Switzerland: vdf Hochschulverlag AG an der ETH Zürich,; 2016. https://doi.org/10.3218/3778-4_23.
[10] Zimmer Henrik, Campen Marcel, Herkrath Ralf, Kobbelt Leif. Variational tangent plane intersection for planar polygonal meshing. In: Hesselgren L, Sharma S, Wallner J, Baldassini N, Bompas P, Raynaud J, editors. Advances in architectural geometry 2012. Vienna: Springer; 2013. p. 319–32. https://doi.org/10.1007/978-3-7091-1251-9_26.
[11] Groenewolt Abel, Schwinn Tobias, Nguyen Long, Menges Achim. An interactive agent-based framework for materialization-informed architectural design. Swarm Intell 2018;12(2):155–86. https://doi.org/10.1007/s11721-017-0151-8.
[12] Pottmann Helmut, Liu Yang, Wallner Johannes, Bobenko Alexander, Wang Wenping. Geometry of multi-layer freeform structures for architecture. p. 65–es ACM Trans Graph 2007;26(3). https://doi.org/10.1145/1276377.1276458.
[13] Rippmann Matthias, Block Philippe. Computational tessellation of freeform, cut-stone vaults. Nexus Netw J 2018;20(3):545–66. https://doi.org/10.1007/s00004-018-0383-y.
[14] Schwinn Tobias, Siriwardena Lasath, Menges Achim. Integrative agent-based architectural design modelling for segmented timber shells. In: Kathrin D, et al., editors. Advances in Architectural Geometry 2023. Berlin, Boston: De Gruyter; 2023. p. 177–92. https://doi.org/10.1515/9783111162683-014 (et al.).
[15] Iuorio Ornella, Korkis Emil, Contestabile Marinella. Digital Tessellation and Fabrication of the ECHO shell. In: Proceedings of the IASS annual symposia. Sixtieth anniversary symposium of the international association for shell and spatial structures structural membranes 2019. Barcelona, Spain: International Association for Shell and Spatial Structures (IASS),; 2019. https://www.ingentaconnect.com/contentone/iass/piass/2019/00002019/00000005/art00012#expand/collapse.
[16] Gabriele Stefano, Varano Valerio, Tomasello Giulia, Alfonsi Davide. R-Funicularity of form found shell structures. Eng Struct 2018;157:157–69. https://doi.org/10.1016/j.engstruct.2017.12.014.
[17] Hawkins Will J, Herrmann Michael, Ibell Tim J, Kromoser Benjamin, Michaelski Alexander, Orr John J, et al. Flexible formwork technologies – a state of the art review. Struct Concr 2016;17(6):911–35. https://doi.org/10.1002/suco.201600117.
[18] Oval Robin, Nuh Mishael, Costa Eduardo, Madyan Omar Abo, Orr John, Shepherd Paul. A prototype low-carbon segmented concrete shell building floor system. Structures 2023;49:124–38. https://doi.org/10.1016/j.istruc.2023.01.063.
[19] Kontovourkis Odysseas, Phocas Marios C, Katsambas Constantinos. Digital to physical development of a reconfigurable modular formwork for concrete casting

and assembling of a shell structure. Autom Constr 2019;106:102855. https://doi.org/10.1016/j.autcon.2019.102855.
[20] Bruun Edvard PG, Ting Ian, Adriaenssens Sigrid, Parascho Stefana. Human–robot collaboration: a fabrication framework for the sequential design and construction of unplanned spatial structures. Digit Creat 2020;31(4):320–36. https://doi.org/10.1080/14626268.2020.1845214.
[21] Stefana Parascho, Augusto Gandia, Ammar Mirjan, Fabio Gramazio, Matthias Kohler, Cooperative fabrication of spatial metal structures. In: Fabricate 2017; 2017, UCL Press: Stuttgart, Germany. Available from: doi: 10.3929/ethz-b-000219566.
[22] Wagner Hans Jakob, Alvarez Martin, Groenewolt Abel, Menges Achim. Towards digital automation flexibility in large-scale timber construction: integrative robotic prefabrication and co-design of the BUGA Wood Pavilion. Constr Robot 2020. https://doi.org/10.1007/s41693-020-00038-5.
[23] Bechert Simon, Sonntag Daniel, Aldinger Lotte, Knippers Jan. Integrative structural design and engineering methods for segmented timber shells - BUGA Wood Pavilion. Structures 2021;34:4814–33. https://doi.org/10.1016/j.istruc.2021.10.032.
[24] Iuorio Ornella. Learning from the past to build the future: multidisciplinary design process. TECHNE J Technol Archit Environ 2021;(21):276–84. https://doi.org/10.13128/techne-9858.
[25] Robeller Christopher, Konaković Mina, Dedijer Mira, Pauly Mark, Weinand Yves. Double-layered timber plate shell. Int J Space Struct 2017;32(3-4):160–75. https://doi.org/10.1177/0266351117742853.
[26] Robeller Christopher, Von Haaren Niklas. Recycleshell: wood-only shell structures made from cross-laminated timber (CLT) production waste. J Int Assoc Shell Spat Struct 2020;61(2):125–39. https://doi.org/10.20898/j.iass.2020.204.045.
[27] Erwin Coumans, Bullet physics simulation. In: ACM SIGGRAPH 2015 Courses. 2015, Association for Computing Machinery: Los Angeles, California. p. Article 7. Available from: doi: 10.1145/2776880.2792704.
[28] Gene Ting-Chun Kao, Axel Körner, Daniel Sonntag, Long Nguyen, Achim Menges, Jan Knippers, Assembly-aware design of masonry shell structures: a computational approach. In: Proceedings of the IASS Annual Symposium 2017; 2017: Hamburg, Germany. Available from: doi: 10.3929/ethz-b-000554318.
[29] Chung Se-Joon, Pollard Nancy. Predictable behavior during contact simulation: a comparison of selected physics engines. Comput Animat Virtual Worlds 2016;27(3-4):262–70. https://doi.org/10.1002/cav.1712.
[30] Heyman Jacques. The stone skeleton. Int J Solids Struct 1966;2(2):249–79. https://doi.org/10.1016/0020-7683(66)90018-7.
[31] Angelillo Maurizio, Fortunato Antonio, Gesualdo Antonio, Iannuzzo Antonino, Zuccaro Giulio. Rigid block models for masonry structures. Int J Mason Res Innov 2018;3:349. https://doi.org/10.1504/IJMRI.2018.095701.
[32] Cascini Lucrezia, Gagliardo Raffaele, Portioli Francesco. LiABlock_3D: a software tool for collapse mechanism analysis of historic masonry structures. Int J Archit Herit 2020;14(1):75–94. https://doi.org/10.1080/15583058.2018.1509155.
[33] Rossi Michela, Calderini Chiara, Di Napoli Beatrice, Cascini Lucrezia, Portioli Francesco. Structural analysis of masonry vaulted staircases through rigid block limit analysis. Structures 2020;23:180–90. https://doi.org/10.1016/j.istruc.2019.10.015.
[34] Livesley Robert K. Limit analysis of structures formed from rigid blocks. Int J Numer Methods Eng 1978;12(12):1853–71. https://doi.org/10.1002/nme.1620121207.
[35] Kao Gene Ting-Chun, Iannuzzo Antonino, Coros Stelian, Van Mele Tom, Block Philippe. Understanding the rigid-block equilibrium method by way of mathematical programming. Proc Inst Civ Eng Eng Comput Mech 2021;174(4):178–92. https://doi.org/10.1680/jencm.20.00036.
[36] Wang Jingwen, Liu Wenjun, Kao Gene Ting-Chun, Mitropoulou Ioanna, Ranaudo Francesco, Block Philippe, et al. Multi-robotic assembly of discrete shell structures. In: Kathrin D, et al., editors. Advances in architectural geometry 2023. Berlin, Boston: De Gruyter; 2023. p. 261–74. https://doi.org/10.1515/9783111162683-020 (et al.).
[37] Latombe Jean-Claude, Wilson Randall H, Gazals Frédéric. Assembly sequencing with toleranced parts. Comput-Aided Des 1997;29(2):159–74. https://doi.org/10.1016/s0010-4485(96)00044-9.
[38] Jiménez Pablo. Survey on assembly sequencing: a combinatorial and geometrical perspective. J Intell Manuf 2013;24(2):235–50. https://doi.org/10.1007/s10845-011-0578-5.
[39] Wilcock Sam, Boyle Jordan H, Dogar Mehmet, Iuorio Ornella. Automated robotics agents for assembly-aware design of shells. In: Proceedings of the Fifth international conference on structures and architecture. Aalborg, Denmark: CRC Press,; 2022. https://doi.org/10.1201/9781003023555-127.
[40] Huang Yijiang, Garrett Caelan R, Ting Ian, Parascho Stefana, Mueller Caitlin T. Robotic additive construction of bar structures: unified sequence and motion planning. Constr Robot 2021;5(2):115–30. https://doi.org/10.1007/s41693-021-00062-z.
[41] Bruno Luca, Gabriele Stefano, Grande Ernesto, Imbimbo Maura, Laccone Francesco, Marmo Francesco, et al. Exploring new frontiers in gridshell design: the FreeGrid benchmark. Structures 2023;58:105678. https://doi.org/10.1016/j.istruc.2023.105678.
[42] Piker Daniel. Kangaroo: form finding with computational physics. Archit Des 2013;83(2):136–7. https://doi.org/10.1002/ad.1569.
[43 Mario Deuss, Anders Holden Deleuran, Sofien Bouaziz, Bailin Deng, Daniel Piker, Mark Pauly, ShapeOp—a robust and extensible geometric modelling paradigm. In: Proceedings of the Modelling Behaviour: Design Modelling Symposium 2015, {C}M. R. Thomsen{C}, et al., Editors; 2015, Springer International Publishing: Cham. p. 505–15. Available from: DOI: 10.1007/978–3-319–24208-8_42.
[44] Grünbaum Branko, Shephard Geoffrey C. The ninety-one types of isogonal tilings in the plane. Trans Am Math Soc 1978;242(0):335–53. https://doi.org/10.1090/s0002-9947-1978-0496813-3.
[45] Gavriil Konstantinos, Schiftner Alexander, Pottmann Helmut. Optimizing B-spline surfaces for developability and paneling architectural freeform surfaces. Comput-Aided Des 2019;111:29–43. https://doi.org/10.1016/j.cad.2019.01.006.
[46] Vestartas Petras, Rad Aryan Rezaei. NGon: Tool for mesh processing and engineering design 2021. https://doi.org/10.5281/zenodo.4550592.
[47] Wilcock Sam, Dogar Mehmet, Iuorio Ornella. Methodology for stability assessment of discretised shell structures during robotic assembly (et al.). In: Gabriele S, editor. Italian workshop on shell and spatial structures. Turin, Italy: Springer; 2023. https://doi.org/10.1007/978-3-031-44328-2_49.
[48] Rezaei Rad Aryan, Burton Henry, Rogeau Nicolas, Vestartas Petras, Weinand Yves. A framework to automate the design of digitally-fabricated timber plate structures. Comput Struct 2021;244:106456. https://doi.org/10.1016/j.compstruc.2020.106456.
[49] Argento Gloria Rita, Gabriele Stefano, Varano Valerio. R-Funicularity of shells and effective eccentricity: influence of tensile strength. Theoretical and Applied Mechanics - AIMETA 2022. Palermo, IT: Materials Research Forum,; 2022. https://doi.org/10.21741/9781644902431-21.
[50] Hu Wengang, Yu Runzhong, Luo Mengyao, Konukcu Arif Caglar. Study on tensile strength of single dovetail joint: experimental, numerical, and analytical analysis. Wood Mater Sci Eng 2023;18(4):1478–86. https://doi.org/10.1080/17480272.2022.2155872.
[51] Kao Gene Ting-Chun, Iannuzzo Antonino, Thomaszewski Bernhard, Coros Stelian, Van Mele Tom, Block Philippe. Coupled rigid-block analysis: stability-aware design of complex discrete-element assemblies. Comput-Aided Des 2022;146:103216. https://doi.org/10.1016/j.cad.2022.103216.
[52] Gene Ting-Chun Kao, COMPAS CRA: Coupled Rigid-Block Analysis (CRA) for the COMPAS framework; 2022.
[53] Sam Wilcock, my_cra_solve.py. 2023: Mendeley data. Available from: doi: 10.17632/sxvsr6yvhy.1.
[54] Şirin Şenol, Aslan Enes, Akincioğlu Gülşah. Effects of 3D-printed PLA material with different filling densities on coefficient of friction performance. Rapid Prototyp J 2023;29(1):157–65. https://doi.org/10.1108/RPJ-03-2022-0081.
[55] Marmo Francesco, Perricone Valentina, Cutolo Arsenio, Carnevali Maria Daniela Candia, Langella Carla, Rosati Luciano. Flexible sutures reduce bending moments in shells: from the echinoid test to tessellated shell structures. R Soc Open Sci 2022;9(5). https://doi.org/10.1098/rsos.211972.